nature communications

Article

https://doi.org/10.1038/s41467-025-65911-9

Quantum teleportation with dissimilar quantum dots over a hybrid quantum network

Received: 27 January 2025

Accepted: 27 October 2025

Published online: 17 November 2025

Check for updates

Alessandro Laneve[1] ✉, Giuseppe Ronco[1], Mattia Beccaceci[1], Paolo Barigelli[1], Francesco Salusti[2], Nicolas Claro-Rodriguez[2], Giorgio De Pascalis[1], Alessia Suprano[1], Leone Chiaudano[1], Eva Schöll[2,3], Lukas Hanschke[2,4], Tobias M. Krieger[3], Quirin Buchinger[5], Saimon F. Covre da Silva[3,6], Julia Neuwirth[1], Sandra Stroj[7], Sven Höfling[5], Tobias Huber-Loyola[5,8,9], Mario A. Usuga Castaneda[10], Gonzalo Carvacho[1], Nicolò Spagnolo[1], Michele B. Rota[1], Francesco Basso Basset[1,11], Armando Rastelli[3], Fabio Sciarrino[1], Klaus D. Jöns[2] & Rinaldo Trotta[1] ✉

Photonic quantum information processing in metropolitan quantum networks lays the foundation for cloud quantum computing, secure communication, and the realization of a global quantum internet. This paradigm shift requires on-demand and high-rate generation of flying qubits and their quantum state teleportation over long distances. Despite the last decade has witnessed an impressive progress in the performances of deterministic photon sources, the exploitation of distinct quantum emitters to implement a quantum relay among distant parties has remained elusive. Here, we overcome this challenge by using dissimilar quantum dots whose electronic and optical properties are engineered by light-matter interaction, multi-axial strain and magnetic fields so as to make them suitable for the teleportation of polarization qubits. This is demonstrated in a quantum network harnessing both fiber connections and a 270 m free-space optical link connecting two buildings of the Sapienza University campus in Rome. The protocol exploits GPS-assisted synchronization, ultra-fast single photon detectors as well as stabilization systems that compensate for atmospheric turbulence. The achieved teleportation state fidelity reaches up to 82 ± 1%, above the classical limit by more than 10 standard deviations. Our field demonstration of all-photonic quantum teleportation opens a new route to implement solid-state based quantum relays and builds the foundation for practical quantum networks.

Large scale quantum networks require the capability of transferring quantum information between distant nodes[1,2]. Currently, photons represent the best candidate to carry out such a task: they are compatible with pre-existing optical fiber[3] and free-space infrastructure[4], they are extremely resilient to environmental decoherence and they feature a variety of easily manipulable degrees of freedom, for which quantum correlations have been demonstrated[5–8]. More specifically, the flexibility and noise resilience of the polarization degree of freedom makes it the current optimal solution to distribute quantum states and quantum correlations over long distances[9,10]. However,

A full list of affiliations appears at the end of the paper. ✉e-mail: alessandro.laneve@uniroma1.it; rinaldo.trotta@uniroma1.it

photon distribution over the globe will inevitably be affected by losses and noise, stressing the need of *quantum relays* and *quantum repeaters*, i.e., “devices" that mitigate the impact of losses by transferring quantum information between distant nodes of a quantum network[11]. These architectures are based on fundamental quantum information protocols such as quantum teleportation and entanglement swapping[12–14], whose successful realization depends on the degree of indistinguishability and entanglement of the involved particles. Thus, the all-photonic implementation of such quantum repeater primitives[15], necessary to efficiently distribute flying qubits, sets stringent requirements on the photon sources to be employed in a quantum network. These include high production rate, wavelength tunability, the need of high photon indistinguishability, and near-unity degree of entanglement, to mention a few. In this perspective, semiconductor quantum dots (QDs) have been under the spotlight for two decades, mainly due to the lack of trade-off between brightness and single photon purity (or degree of entanglement) that is typically plaguing Poissonian sources of light[16]. More specifically, QDs have shown on-demand generation of single and entangled photons with high indistinguishability[17,18], near-unity degree of entanglement[19], ultra-low multi-photon emission[20] and, most importantly, high brightness[21–23]. For this reason, and for their compatibility with quantum memories[24–26], semiconductor QDs have been acknowledged as a promising candidate to become the ideal quantum light source for quantum networking[16,27,28]. Following this direction, QDs have been employed for successful demonstrations of photonic quantum teleportation and entanglement swapping using a single emitter (including emitters in the telecommunication band)[29–36], even using non-ideal devices[37]. Moreover, two distinct QDs have been interfaced to achieve quantum teleportation from a photonic qubit to a spin qubit[38], and distinct QD spin qubits have been made entangled through a heralded protocol[39]. Nonetheless, the use of independent QDs to implement all-photonic quantum teleportation in a quantum relay scenario demands state-of-the-art sources of both single and entangled photons to be interfaced via two-photon interference. This, in turn, requires the indistinguishability of photons generated by independent QDs, which inevitably feature dissimilar optical properties. Although pioneering steps along this direction have been moved[18,38,40–43], the implementation of quantum relays interfacing distinct QDs has remained elusive because of the complexity of realizing a device that meets all the requirements set by all-photonic teleportation at the same time. Indeed, achieving efficient generation of single and entangled photons from QDs requires the use of sophisticated nanophotonic devices[44–46] that exploit light-matter interaction to boost the flux of QD photons. Moreover, since QDs are to deliver highly entangled photons, their electronic structure has to be controlled with high accuracy[47–49].

Here, we overcome these limitations by combining a variety of cutting-edge techniques developed in the context of QD quantum photonics. We fabricate state-of-the-art semiconductor QDs deterministically embedded in Circular Bragg Resonators (CBRs)[23,50], designed to enhance the collection efficiency of both single and entangled photon pairs[51]. Then, we integrate them onto piezoelectric actuators to enable energy tunability and FSS erasing[51]. We use external perturbations, specifically multi-axial strain and magnetic fields, to reshape the electronic structure of dissimilar QDs so as to make them suitable for quantum teleportation. Finally, we take advantage of ultrafast nanowire single photon detectors to mitigate the effects of residual photon distinghuishability. These tools enable the demonstration of all-photonic quantum state teleportation with separate and originally dissimilar QDs. In addition, we manage to implement this protocol in an urban communication scenario, distributing teleported photons in a hybrid quantum network (composed of both fiber and free-space links) built over the campus of Sapienza University in Rome[52,53].

Results

The quantum teleportation scheme and setup is showcased in Fig. 1. Two independent and remote QDs are driven under two-photon resonant excitation (TPE)[54] to generate nearly on-demand photon pairs through the biexciton-exciton radiative cascade[55]. We denote the photon emitted by the biexciton recombination as XX, and the one after the exciton recombination as X (Fig. 1a). The input state $|\phi\rangle$ is prepared in the polarization degree of freedom of the X_1 photons, generated by QD_1 in a first laboratory, acting as Node 1 (see Fig. 1b). This photon is sent to a second laboratory, Node 2, where QD_2 generates the XX_2-X_2 entangled photon pair. There, the quantum interference between X_1 and X_2 photons enables the teleportation of the $|\phi\rangle$ target state onto the polarization state of XX_2, which is entangled to X_2. We first benchmark the teleportation between the two separated nodes 1 and 2 in the Marconi building of the Sapienza Physics Department, realizing a demonstration of all-photonic quantum teleportation between photons emitted by distinct QDs. Then, the XX_2 photon is sent via a 270 m free-space optical link to a third laboratory in a different building of the campus (named after Fermi), acting as Node 3. The link is equipped with specifically designed synchronization devices, and stabilization systems to compensate for atmospheric turbulence. Overall, we achieve the successful teleportation of a polarization qubit using dissimilar QDs in an urban quantum network comprising both fiber and free-space links. The key to the success of the experiments lies in the use of state-of-the-art photonic cavities in combination with quantum-engineering techniques (as sketched in Fig. 1b) to make QD_1 and QD_2 suitable for quantum teleportation, as explained in the next section.

Engineering quantum light sources

For a successful all-photonic quantum teleportation with two remote QDs, three fundamental ingredients are required: *(i)* a bright source of highly entangled photon pairs; *(ii)* a bright source of single photons with tunable energy; *(iii)* the capability to perform a successful Bell state measurement (BSM). We accomplish *(i)* by using state-of-the-art epitaxial GaAs quantum dots fabricated by the droplet etching method[56]. They can act as bright and reliable sources of single and highly polarization-entangled photon pairs, especially when embedded in suitable photonic structures[23]. In our case, we employ GaAs QDs coupled to CBRs, also known as bullseye cavities, in turn integrated onto micromachined piezoelectric actuators made of $[Pb(Mg_{\frac{1}{3}}Nb_{\frac{2}{3}})O_3]_{0.72}$-$[PbTiO_3]_{0.28}$ (PMN-PT)[51], as depicted in Fig. 2a. The CBR cavity engineers light-matter interaction to boost the flux of both X and XX photons generated during the radiative cascade. Single-photon (photon-pair) extraction efficiencies as high as 85% (65%) have been demonstrated with this type of cavity[23]. The micro-machined PMN-PT actuators are instead used to control the QD electronic structure via the application of independent stress fields applied along different crystal directions. These are needed to cancel out the energy splitting between the two X states—the fine structure splitting (FSS)—that is usually induced by asymmetries in the QD confining potential (see Fig. 2b). Erasing this “which-path" information in the radiative cascade is fundamental to obtain near-unity degree of entanglement without temporal post-selection[47,49,51]. In our experiment we employ PMN-PT in combination with CBR cavities: by varying the voltages applied to the piezoelectric actuators, we reach a minimum value of $FSS = 0.3 \pm 0.2\ \mu eV$ for QD_2, as reported in Fig. 2b. By performing quantum state tomography on the generated photon pairs we estimate a fidelity of $F = 0.94 \pm 0.01$ to the $|\phi^+\rangle$ Bell state without resorting to any time-filtering procedure (see Fig. 2c), close to the best obtained with QDs in optical microcavities[51]. The source of the teleported qubit *(ii)* is another GaAs QD embedded in a CBR cavity, denoted as QD_1 (Fig. 2d), driven under TPE and generating X_1 and XX_1 photons. The latter are not relevant for the teleportation protocol discussed here

https://doi.org/10.1038/s41467-025-65911-9

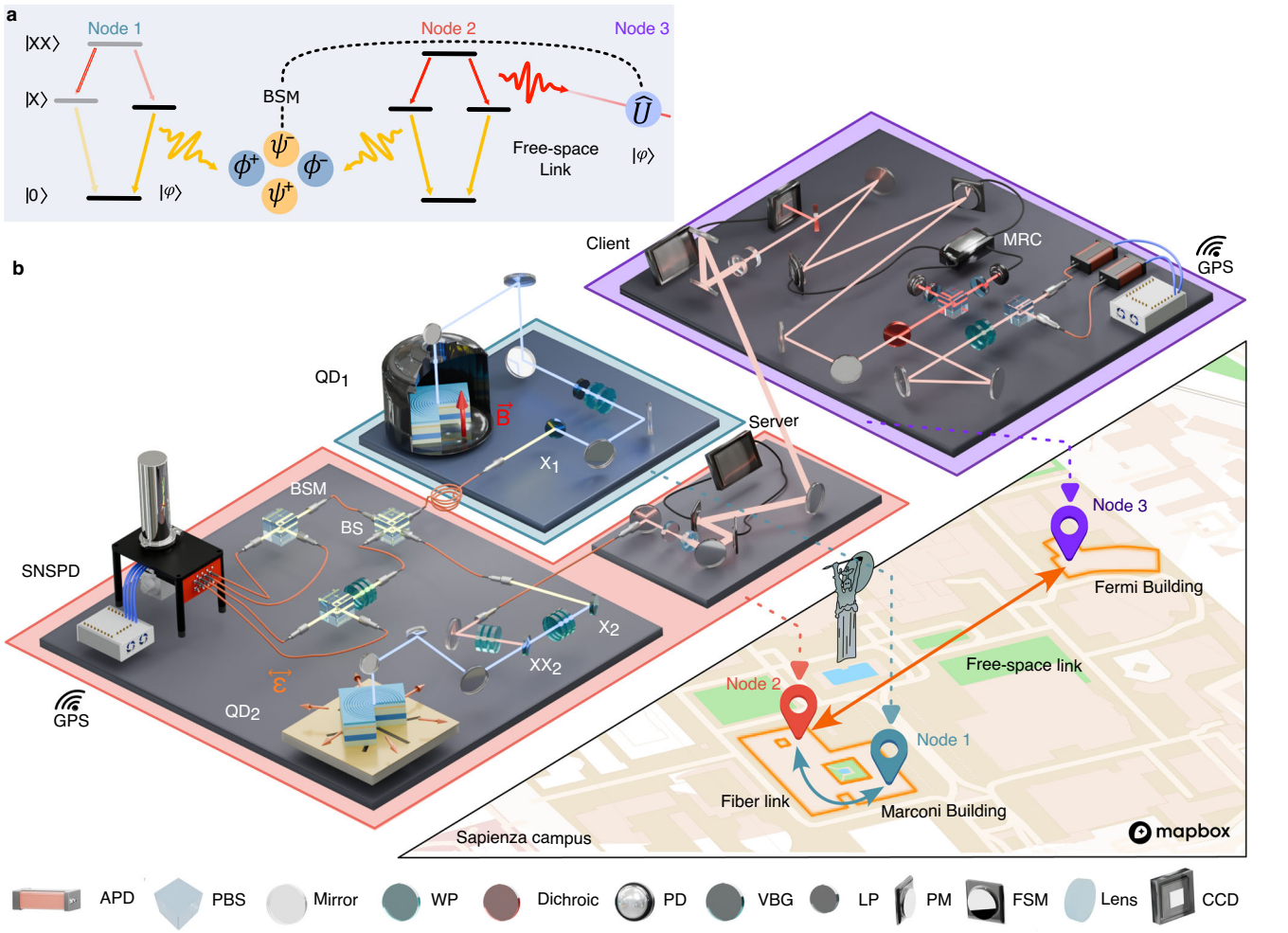

Fig. 1 | Sketch of the urban quantum teleportation network. a Scheme of the quantum teleportation protocol as implemented with two QDs over a network including a free-space link. **b** Depiction of the teleportation experimental realization over the Sapienza University campus. In Node 1, highlighted in teal and placed in the Marconi building, the X_1 photon from QD_1 is selected and prepared in a well-defined polarization state. Node 1 is connected with a 15 m optical fiber link to Node 2, highlighted in red, where QD_2 emits a polarization-entangled biexciton-exciton photon pair, XX_2 and X_2. Spatial displacement between Node 1 and Node 2 is accentuated on the map for clarity. A BSM is performed in Node 2, while XX_2 is sent to Node 3, highlighted in purple and placed in the Fermi building, through a 270 m free-space optical link. The strain and the magnetic field harnessed to optimize the X_2-XX_2 degree of entanglement and the X_1 emission wavelength, are featured in orange and red, respectively. The experimental setup accommodates Volume-Bragg Gratings (VBGs), polarizing beam-splitters (PBSs), waveplates (WPs), linear polarizers (LPs), avalanche single photon detectors (APDs), piezoelectric mirrors (PMs), fast steering mirrors (FSMs), photodiodes (PDs) and client-server PCs for the optimization of the free-space optical link. Inset: map depicting the hybrid quantum network laid over the Sapienza campus, where the Marconi and Fermi buildings are framed in orange. Map data from © Mapbox, © OpenStreetMap.

and they will not be considered further. The X_1 photon features a wavelength similar to X_2 - but not identical, as we report in detail in the "Methods" section. This is a clear indication that the two independent QDs feature slightly different size, shape or alloy intermixing[57]. In order to achieve spectral indistinguishability between X_1 and X_2, we employ a magnetic field that shifts the emission by the combination of Zeeman splitting and diamagnetic shift. More specifically, we select one of the Zeeman-split X_1 transitions and use the magnetic field to tune its energy in resonance with the X_2 photon, as reported in in Fig. 2e. This step is crucial to achieve *(iii)*. In its most efficient implementation with linear optics, a BSM exploits two photons that interfere on a symmetric beam splitter (BS) coming from two distinct input ports. Then, they undergo a polarization projective measurement at the two output ports, allowing to sample two of the four Bell states, $|\psi^+\rangle = \frac{|HV\rangle+|VH\rangle}{\sqrt{2}}$ and $|\psi^-\rangle = \frac{|HV\rangle-|VH\rangle}{\sqrt{2}}$. To perform a successful BSM, the impinging photons have to be indistinguishable in all degrees of freedom. While the magnetic field tuning allows us to achieve energetic resonance, X_1 and X_2 feature also different lifetimes and linewidths, a consequence of a slightly different Purcell acceleration as well as different interaction with the solid-state environment. This can be indirectly observed in the Hong-Ou-Mandel (HOM) interference measurement of X_1-X_2 photon pairs (realized by performing cross- and co-polarized interference, see the inset of Fig. 2f), exhibiting the typical "volcano shape"[58,59]. Collecting all the photons coming out from the BS results in a limited HOM visibility, an evidence which can be fully explained by the lifetimes and linewidths of the X_1 and X_2 photons (see the SI). However, the level of indistinghuishability can be improved by post-selecting two-photon interference events via ultrafast superconductive nanowire single photon detectors (SNSPDs) with a temporal resolution <15 ps (FWHM) and a time-to-digital converter with 19 ps time resolution (FWHM), resulting in a total setup time resolution of around 24 ps (FWHM) for coincidences. By narrowing down the considered coincidence detection window $\Delta\tau$, we can achieve HOM visibilities as high as 60% (see Fig. 2f), a value limited by the SNSPDs time resolution. This technique clearly comes at the cost of the number of useful three-fold coincidences exploitable for the teleportation protocol, but not as much as

https://doi.org/10.1038/s41467-025-65911-9

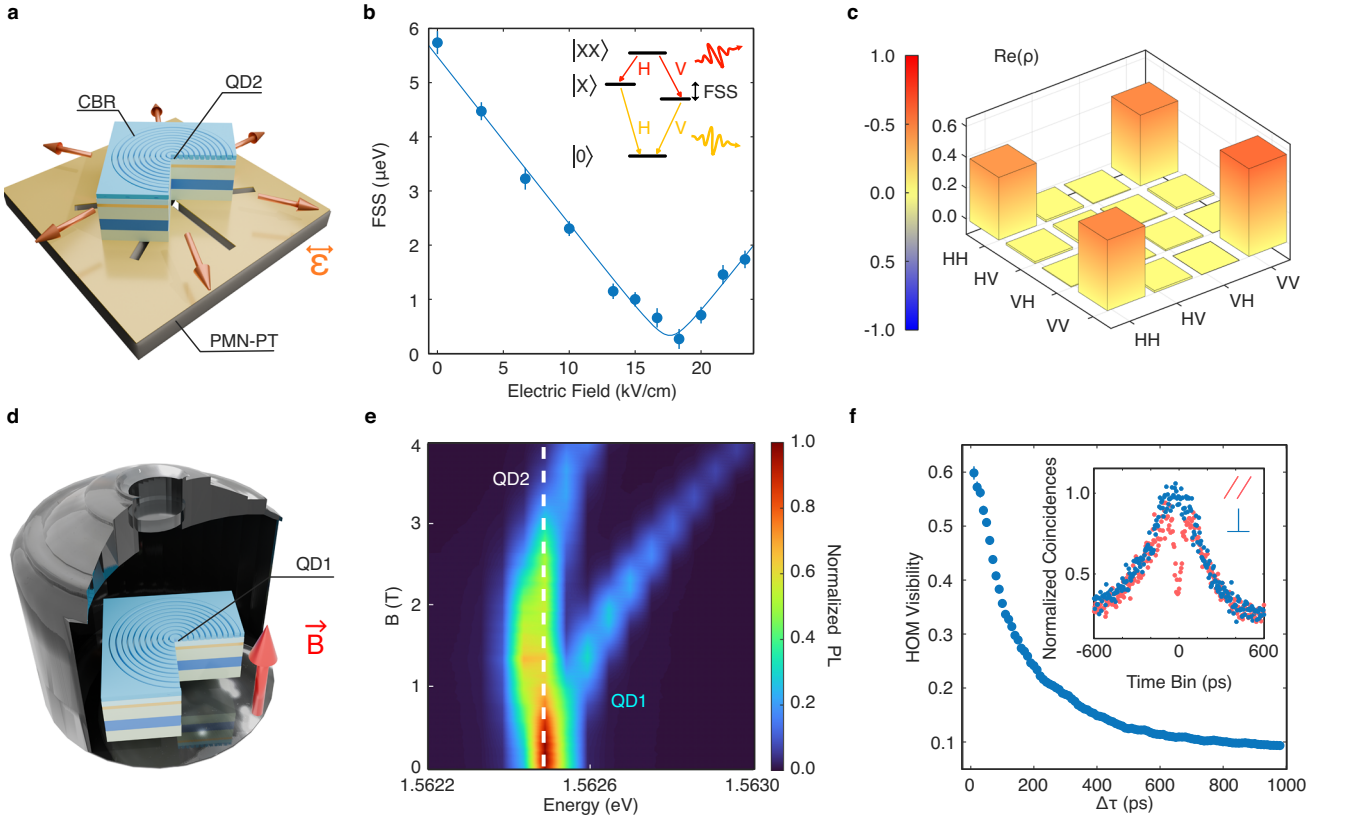

Fig. 2 | Quantum resources engineering. a Schematic representation of the CBR QD_2 integrated onto PMN-PT to enable the application of mechanical stress. **b** The strain-tuning curve along one axis showing our capability to erase the FSS. The solid line is a fit from the model equations reported in ref. 48. **c** Experimental two-photon density matrix (real part) measured for FSS = 0.3 ± 0.2 μeV, yielding a fidelity $F_{|\phi^+\rangle} = 0.94 \pm 0.01$ and a concurrence $C = 0.89 \pm 0.01$. **d** Schematic representation of QD_1 inserted in a magneto-cryostat. **e** Diamagnetic shift and Zeeman splitting of the emission spectrum of QD_1: thanks to a fine tuning of the B intensity, we achieve spectral overlap between the two X photons applying a magnetic field of $B = 0.9$ T. **f** HOM visibility between photons from remote QDs as a function of the coincidence time window $\Delta\tau$, setting the magnetic field at $B = 0.9$ T: post-selection on the HOM events allows us to reach a maximum HOM visibility of $V_{HOM} = 0.598 \pm 0.025$ for a 20 ps time window. It is worth noting that the overall time resolution of the setup adds up to 24 ps. Inset: time histogram of coincidences in the HOM experiment for co-polarized photon pairs (red) and cross-polarized photon pairs (blue) at the optimal $B = 0.9$ T.

one would intuitively expect. In fact, we point out that the teleportation fidelity that can be achieved in an experiment depend on both the degree of entanglement and photon-indistinghuishability, and overcoming the classical limit is possible even if the available quantum resources are unbalanced, i.e., even with imperfect and dissimilar quantum dots. We have explored this possibility by using a model that computes the maximum theoretically achievable teleportation fidelity F_T as a function of the degree of entanglement in the X_2-XX_2 photon pair (which is influenced by FSS and quantified by the fidelity of the photon pair state to the $|\phi^+\rangle$ Bell state) and the indistinguishability of the X_1-X_2 photons (measured by their HOM visibility). F_T is computed considering the fidelity $F = \langle\phi|\rho_{\prime}|\phi\rangle$ of the teleported state $\rho_{\prime}$ to the expected output state $|\phi\rangle$ for a perfect teleportation, and averaging over the set of possible input states. The details of the model are reported in the SI while the achieved results are illustrated in Fig. 3a. For the characteristics of our emitters and a BSM coincidence time window of 30 ps, the predicted teleportation fidelity is $F_T = 0.827 \pm 0.006$, represented by a white star in Fig. 3a. Most importantly, the same figure highlights that the classical limit can be overcome even with a poor HOM visibility (below 20%) in combination with a high level of Bell state fidelity (above 90%). This suggests that successful teleportation with our independent QDs can be achieved by a loose temporal post-selection, at moderate expenses of teleportation rates. This is exactly what motivated our field demonstration of quantum teleportation, as presented in the next section.

Teleportation protocol over a quantum network

The protocol we used builds upon the scheme employed in one of the seminal demonstration of quantum teleportation[60]. We perform the experiment by preparing X_1 photons in the target polarization states $|\phi\rangle$ in Node 1 and sending them through a 15 m single-mode fiber to Node 2, where they interfere with the X_2 photons through the BSM. At the same time, the XX_2 photons undergo a polarization measurement in Node 2, where we collect the three-fold coincidences among their detection and X_1-X_2 coincidence events in the chosen projection of the BSM. After the X_1-X_2 interference, the joint polarization state of X_1-X_2-XX_2 can be written as[61]:

$$|\Psi\rangle = \frac{1}{2}\Big(|\phi^+\rangle_{X_1,X_2}\hat{I} + |\psi^+\rangle_{X_1,X_2}\hat{\sigma}_X + -i|\psi^-\rangle_{X_1,X_2}\hat{\sigma}_Y + |\phi^-\rangle_{X_1,X_2}\hat{\sigma}_Z\Big)|\phi\rangle_{XX_2} \quad (1)$$

where $\hat{I}$ is the identity operator and $\hat{\sigma}_{X/Y/Z}$ are the Pauli operators. The BSM projection on one of the two Bell states $|\psi^-\rangle$ and $|\psi^+\rangle$ corresponds to the application of a different operation to the teleported qubit. The entire teleportation protocol from X_1 to XX_2 can be fully characterized by performing a quantum process tomography (QPT)[62], which produces the *process matrix*. By collecting three-fold coincidences for different input states, we can reconstruct the teleportation process matrix for different values of BSM coincidence time window $\Delta\tau$. Those are reported for both projections and $\Delta\tau = 30$ ps in

https://doi.org/10.1038/s41467-025-65911-9

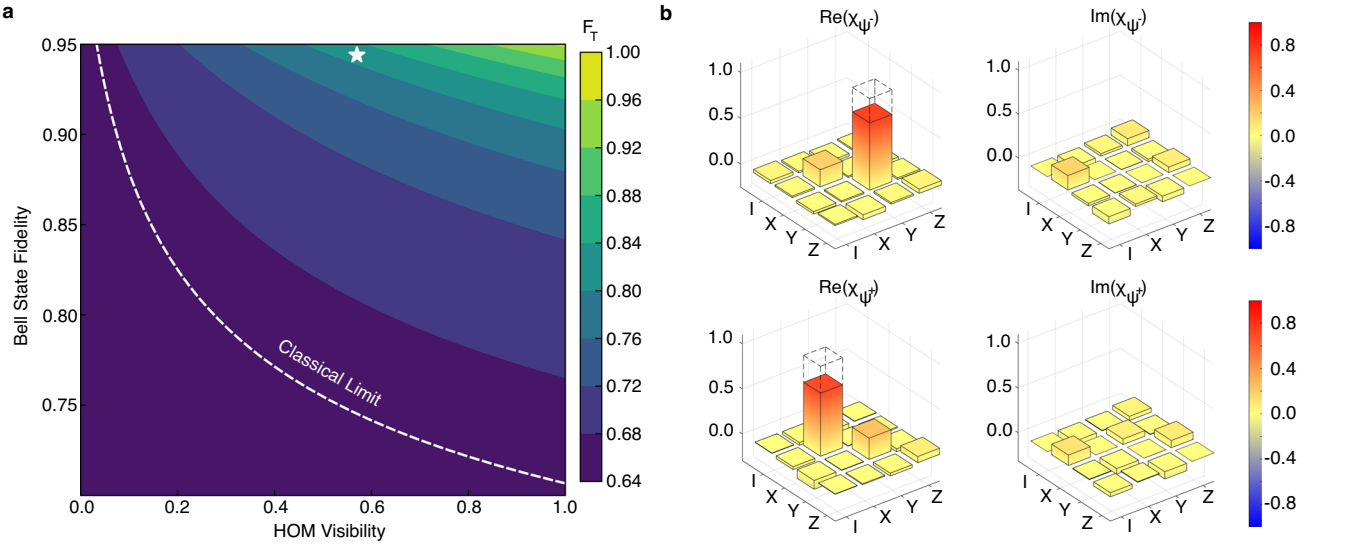

Fig. 3 | Quantum state teleportation. a Theoretical teleportation fidelity as a function of the quantum resources available for the protocol, computed for the case of a 50% BSM. The white curve highlights the maximum achievable fidelity with classical resources, i.e., for a protocol only relying on classical correlations. The white star points out the expected teleportation fidelity as estimated with our theoretical model. In particular, our Bell state fidelity is 0.94 ± 0.01 and the HOM visibility for 30 ps coincidence window is $V_{HOM} = 0.57 \pm 0.02$, yielding an average teleportation fidelity $F_T = 0.827 \pm 0.006$. **b** Experimental process matrices $\chi_{\psi^{+/-}}$ for the teleportation protocol, as defined in ref. 62, reported both for the projection on $|\psi^-\rangle$ (top) and $|\psi^+\rangle$ (bottom), and in comparison with the corresponding ideal process matrix (dashed). The matrices are represented in terms of the quantum operations I (the identity), $X = \sigma_X$, $Y = -i\sigma_Y$ and $Z = \sigma_Z$, where $\{\sigma_{X/Y/Z}\}$ are the Pauli matrices.

Fig. 3b. From these matrices, we estimate the overall teleportation fidelity which is found to be $F_T^- = 0.82 \pm 0.01$ for the $|\psi^-\rangle$ projection and $F_T^+ = 0.77 \pm 0.01$ for the $|\psi^+\rangle$ one.

Both values are well above the classical limit of $\frac{2}{3}$[63] by more than 10 standard deviations. Yet, it is worth noting that in the $|\psi^+\rangle$ projection case we do not reach the theoretical limit of $F_T = 0.827 \pm 0.006$ estimated for our QDs. This is due to hardly avoidable setup imperfections and other sources of undesired background signal. In particular, we estimate that a slightly imperfect polarization compensation procedure may have decreased the teleportation fidelity for the $|\psi^+\rangle$ projection of around 2%. We provide further discussion of these points in the SI. As mentioned above, our scheme uses temporal post-selection and we investigate how the teleportation fidelity changes as a function of $\Delta\tau$. The red plot in Fig. 4 displays the teleportation results averaged over the $|\psi^-\rangle$ and $|\psi^+\rangle$ projections applying different coincidence time windows to the BSM up to $\Delta\tau = 30$ ps. It can be clearly seen that the classical limit can be overcome by a relatively moderate temporal post-selection, with a $\Delta\tau$ of about 200 ps. This value allows to retain more than 60% of the total three-fold coincidence events, corresponding to ≈0.5 Hz rate of teleportation events. The best teleportation fidelity is obtained for the $\Delta\tau = 30$ ps window, which allows to retain about 11% of the total teleportation events, corresponding to a ≈0.1 Hz teleportation rate. These results stimulated us to explore the possibility to implement our teleportation scheme in an urban communication scenario, specifically using the Sapienza free-space link[52,53]: a 270 m free-space channel laid over the university campus in the city center of Rome. Rather than being locally analyzed, XX_2 photons are sent through the quantum channel and measured in Node 3, in the Fermi building of Sapienza. This operation presents many challenges, including the presence of substantial losses (almost 90% of the signal is lost through the channel), the need to synchronize photon detection, as well as the presence of atmospheric turbulence which makes the coupling of the signal to single-mode fibers unstable. The synchronization and instability issues are alleviated by the employment of GPS disciplined oscillators and a stabilization system based on both slow and fast steering mirrors, respectively[52]. The results are shown in Fig. 4, where we report the teleportation fidelities we obtain for a given $\Delta\tau$, in comparison with those achieved in the fiber-only network (see SI for details). Given the losses present in the free-space link, the uncertainty on the fidelity values is considerably larger with respect to the fiber-only network. However, for $\Delta\tau = 30$ ps, we obtain an average teleportation fidelity of $F_T = 0.80 \pm 0.04$, more than 3σ above the classical limit. The slightly lower teleportation fidelities that can be observed in the hybrid network are related to the presence of the free-space channel, which favors the teleportation of some polarization states in comparison with others, due to imperfect polarization compensation procedures. We discuss these points in more detail in the SI.

Discussion

In this work, we demonstrate all-photonic quantum state teleportation using photons generated by two independent and dissimilar quantum emitters, specifically epitaxial QDs. Although our results are still not comparable to those achievable with single photons from SPDC and weak coherent pulses, in terms of joint fidelity and success rate[64–67], we managed to exploit solid-state deterministic emitters to realize a quantum relay, while also successfully implementing the protocol in an urban quantum network that presents several challenges, including photon losses, atmospheric turbulence, and the need of synchronizing different nodes. We achieve this results by overcoming some of the roadblocks that have long prevented the implementation of a fully photonic quantum teleportation with quantum emitters. The key to this accomplishment was the use of strain- and magnetic-field-tunable QDs embedded in nanophotonic cavities and the exploitation of state-of-the-art techniques for single photon detection and event analysis. This allowed us to surpass the classical threshold for state teleportation while retaining more than 60% of the total events rate. Moreover, we recorded an average fidelity of up to $79 \pm 1\%$ for about 11% of the total teleportation events. Our achievement opens an avenue for the development of practical quantum networks and will stimulate additional research endeavors. Furthermore, a contemporary work[68] also realized all-photonic quantum teleportation, using frequency conversion to achieve both the necessary photon indistinguishability and efficient fiber communication[28,41], although at the cost of comparably high noise levels. These results offer a perspective of scalability over

https://doi.org/10.1038/s41467-025-65911-9

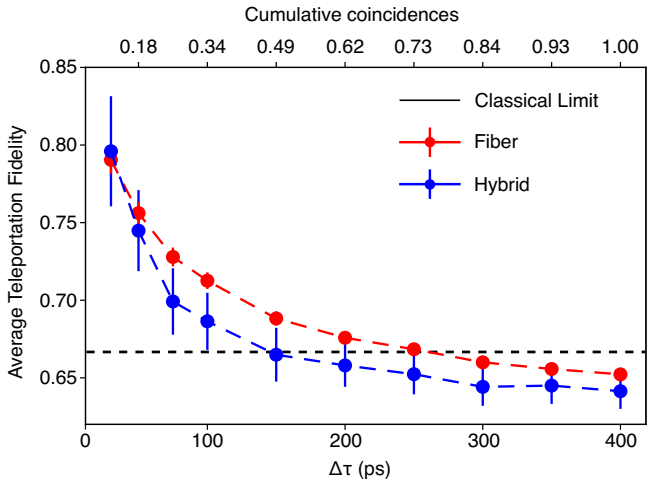

Fig. 4 | Temporal post-selection of quantum teleportation events. Teleportation fidelity averaged over the $|\psi^-\rangle$ and $|\psi^+\rangle$ projections as a function of the BSM coincidence time window $\Delta\tau$. We compare the results obtained for the fiber network case (red points) with the hybrid scenario (blue points), where teleported photons are sent over a 270 m free-space channel. On the top axis, the fraction of retained events over the total (corresponding to a coincidence time window of 400 ps) is reported as a function of $\Delta\tau$.

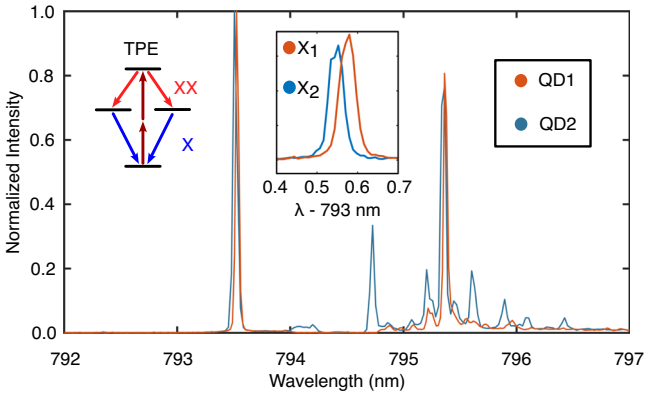

Fig. 5 | Optical properties of the single-photon and entangled photons sources. QD_1 and QD_2 emission spectra for TPE excitation. The emission wavelength of the two excitons X_1 and X_2, even in absence of external tuning, partially overlaps, as shown in the inset.

pre-existing infrastructure that further motivate research in the direction of QD-based networking. This considered, some issues still have to be addressed to reach application-ready performances, but the path is already set for most of them. For instance, several approaches can be put in place to reach near-unity teleportation fidelities at the maximum possible rates. First, the implementation of electric fields to suppress charge noise[69] will allow blinking suppression[70] and the improvement of the indistinguishably of photons generated by remote QDs. This possibility has been demonstrated for single photon sources[18], but additional efforts are still needed to improve the brightness of the devices and extend the method to entangled photon sources. Recent results[71] also suggest that differential Purcell enhancement can be implemented to mitigate photon distighuishability arising from time-correlation between XX and X photons[59]. Regarding the free-space link, the integration of adaptive optics for compensation of high-order aberrations due to atmospheric turbulence as well as the use of efficient synchronization strategies may allow reducing photon losses to the minimum possible. We can also envision a combination with a frequency conversion approach to enable deployed fiber communication, although a significant improvement in noise levels and efficiency would be required to grant performances comparable to in-lab results. The realization of a QD-based quantum relay also represents a step towards the demonstration of entanglement swapping with remote QDs, and then, given the well-established compatibility between QD emitters and efficient quantum memories, the realization of a quantum repeater based on QD emitters. The requirements on the light sources are more stringent in this case, but our results provide a strong indication that the realization of the protocol is within sight. More in general, our demonstration of quantum teleportation in an urban communication scenario highlights that the implementation of a QD-based quantum network for quantum information processing is a likely perspective in the foreseeable future.

Methods

Source characterization

In Fig. 5, we report the normalized spectra of both QDs under resonant two-photon excitation. Even without the application of an external magnetic field, we already observe a partial overlap between the exciton emission lines (see inset of Fig. 5). We measure a multiphoton emission probability for the three transitions of $g^{(2)}_{X_1}(0) = 0.013 \pm 0.001$, $g^{(2)}_{X_2}(0) = 0.016 \pm 0.001$ and $g^{(2)}_{XX_2}(0) = 0.039 \pm 0.001$. Lifetimes of 100 ± 10 ps, 67 ± 5 ps, and 259 ± 30 ps are measured for X_2, XX_2, and X_1 respectively. Comparison with an unprocessed sample[35] shows a Purcell factor $F_P^{X_2} \approx 2.5$ and $F_P^{XX_2} \approx 1.8$, while X_1 emission rate does not show Purcell enhancement. This unbalance in the excited state lifetimes results in a lower wavepackets overlap between the X photons arriving at the BSM setup, which lowers the degree of indistinguishability[72]. A detailed computation of the expected overlap is provided in the SI. The low Purcell acceleration we record shows that, for our case and in general for CBR cavities employed for photon pair extraction[51], the main advantage coming from coupling the emitter to a nanostructure is represented by the enhanced extraction efficiency. QD_2 exhibits the optimal extraction efficiency reported in ref. 51 ($\eta_{ext}^{pair} = 0.65$ and $\eta_{ext}^{single} \approx 0.85$, much higher than the values achievable with unprocessed emitters[35]), while QD_1 shows a single-photon extraction efficiency a factor 6 lower. Therefore, the brightness of QD_1 limits the protocol performance, yielding an estimated rate of teleportation three-fold events of $\approx 7.8 \times 10^{-6}$ per prepared photon (at the best time filtering of $\Delta\tau = 30$ ps on the BSM). On the other hand, for the same $\Delta\tau = 30$ ps coincidence window, the BSM events rate per prepared photon is $\approx 2 \times 10^{-4}$. In the SI we provide a detailed description of the experimental setup as well as the characterization setup employed to perform the analyses we report above.

Bell state measurement

The quantum teleportation protocol relies on the successful projection of a two-photon polarization state on a Bell state. However, the perfect discrimination between the four Bell states $\{|\phi^+\rangle, |\phi^-\rangle, |\psi^+\rangle, |\psi^-\rangle\}$ is not allowed with local operations and classical communication[73], unless ancillary degrees of freedom or systems are employed[74]. The limit for the efficiency of a BSM implemented by linear optics and no ancillary qubits has been set at 50%[75]. The experimental realization of such projective measurements consists of a HOM interference between the two photons, followed by a polarization-sensitive detection (experimental details are reported in the SI). After HOM interference, photon polarization is measured in the $\{|H\rangle, |V\rangle\}$ basis at both outputs of the interference BS. Thanks to this measurement stage it is possible to perfectly discriminate between $|\psi^-\rangle$ and $|\psi^+\rangle$ by collecting coincidences between orthogonally polarized outputs[36,37], while all the events corresponding to $|\phi^+\rangle = \frac{|HH\rangle + |VV\rangle}{\sqrt{2}}$ and $|\phi^-\rangle = \frac{|HH\rangle - |VV\rangle}{\sqrt{2}}$ produce no conclusive outcome.

Quantum process tomography

To characterize the performances of our protocol, we have performed a complete Quantum Process Tomography (QPT)[76] of our quantum teleportation, depicting it as a quantum channel applied to the input qubit, conditioned on the BSM result. A quantum channel can be represented as a map $\mathcal{E}$ acting on an input state ρ as follows:

$$\mathcal{E}(\rho) = \sum_i E_i \rho E_i^\dagger \tag{2}$$

where the operators E_i satisfy the condition $\sum_i E_i^\dagger E_i = \mathbb{I}$. The E_i operators must be expressed in function of a fixed set of operators $\tilde{E}_k$, which form a basis for the set of operators on the state space: $E_i = \sum_k e_{ik}\tilde{E}_k$. Using this basis, the quantum channel can be expressed as:

$$\mathcal{E}(\rho) = \sum_{mn} \chi_{mn} \tilde{E}_m \rho \tilde{E}_n^\dagger \tag{3}$$

where $\chi_{mn} = \sum_i e_{im} e_{in}^*$ is a positive hermitian matrix defined as the χ-matrix representation of the process $\mathcal{E}$. For the specific case of a single qubit, it is possible to show that choosing the Pauli matrices as the basis operators ($\tilde{E}_0 = I$, $\tilde{E}_1 = \sigma_x$, $\tilde{E}_2 = -i\sigma_y$, $\tilde{E}_3 = \sigma_z$), the χ matrix can be completely determined by measuring the density matrices of the four polarization states $|H\rangle$, $|V\rangle$, $|D\rangle = (|H\rangle + |V\rangle)/\sqrt{2}$ and $|R\rangle = (|H\rangle + i|V\rangle)/\sqrt{2}$ after the action of $\mathcal{E}$[62]. In the SI we report the single-qubit density matrices employed to reconstruct the process matrices in Fig. 3. In order to ensure that our analysis yields physically meaningful results we adopt a Maximum Likelihood Estimation (MLE) algorithm developed for QPT[77]. It is now possible to compute the $\rho' = \mathcal{E}(\rho)$ for the experimental quantum teleportation process and, comparing ρ' with the expected outcome $|\phi\rangle$, by computing the fidelity $F = \langle\phi|\rho'|\phi\rangle$, we can estimate the efficiency of the teleportation. In particular, we average over six possible polarization states $\{|H\rangle, |V\rangle, |D\rangle, |A\rangle = (|H\rangle - |V\rangle)/\sqrt{2}, |R\rangle, |L\rangle = (|H\rangle - i|V\rangle)/\sqrt{2}\}$ to compute F_T, as we explain in detail in the SI.

Data availability

The data supporting the results of this paper are available in the main text and the Supplementary Information. Further data are available from the corresponding authors upon request.

Code availability

The code supporting the analysis reported in this paper is available from the corresponding authors upon reasonable request.

References

1. Kimble, H. J. The quantum internet. *Nature* **453**, 1023 (2008).
2. Wehner, S., Elkouss, D. & Hanson, R. Quantum internet: a vision for the road ahead. *Science* **362**, eaam9288 (2018).
3. Mao, Y. et al. Integrating quantum key distribution with classical communications in backbone fiber network. *Opt. Express* **26**, 6010 (2018).
4. Yin, J. et al. Entanglement-based secure quantum cryptography over 1,120 kilometres. *Nature* **582**, 501 (2020).
5. Kwiat, P. G. Hyper-entangled states. *J. Mod. Opt.* **44**, 2173 (1997).
6. Mair, A., Vaziri, A., Weihs, G. & Zeilinger, A. Entanglement of the orbital angular momentum states of photons. *Nature* **412**, 313 (2001).
7. Simon, C. & Poizat, J.-P. Creating single time-bin-entangled photon pairs. *Phys. Rev. Lett.* **94**, 030502 (2005).
8. Tanzilli, S. et al. A photonic quantum information interface. *Nature* **437**, 116 (2005).
9. Yin, J. et al. Satellite-based entanglement distribution over 1200 kilometers. *Science* **356**, 1140 (2017).
10. Ren, J.-G. et al. Ground-to-satellite quantum teleportation. *Nature* **549**, 70 (2017).
11. Gisin, N. & Thew, R. Quantum communication. *Nat. Photonics* **1**, 165 (2007).
12. Jacobs, B. C., Pittman, T. B. & Franson, J. D. Quantum relays and noise suppression using linear optics. *Phys. Rev. A* **66**, 052307 (2002).
13. Briegel, H.-J., Dür, W., Cirac, J. I. & Zoller, P. Quantum repeaters: the role of imperfect local operations in quantum communication. *Phys. Rev. Lett.* **81**, 5932 (1998).
14. Duan, L.-M., Lukin, M. D., Cirac, J. I. & Zoller, P. Long-distance quantum communication with atomic ensembles and linear optics. *Nature* **414**, 413 (2001).
15. Azuma, K. et al. Quantum repeaters: from quantum networks to the quantum internet. *Rev. Mod. Phys.* **95**, 045006 (2023).
16. Lodahl, P. Quantum-dot based photonic quantum networks. *Quantum Sci. Technol.* **3**, 013001 (2017).
17. Schöll, E. et al. Resonance fluorescence of GaAs quantum dots with near-unity photon indistinguishability. *Nano Lett.* **19**, 2404 (2019).
18. Zhai, L. et al. Quantum interference of identical photons from remote GaAs quantum dots. *Nat. Nanotechnol.* **17**, 829 (2022).
19. Huber, D. et al. Highly indistinguishable and strongly entangled photons from symmetric GaAs quantum dots. *Nat. Commun.* **8**, 15506 (2017).
20. Schweickert, L. et al. On-demand generation of background-free single photons from a solid-state source. *Appl. Phys. Lett.* **112**, 093106 (2018).
21. Dousse, A. et al. Ultrabright source of entangled photon pairs. *Nature* **466**, 217 (2010).
22. Somaschi, N. et al. Near-optimal single-photon sources in the solid state. *Nat. Photonics* **10**, 340 (2016).
23. Liu, J. et al. A solid-state source of strongly entangled photon pairs with high brightness and indistinguishability. *Nat. Nanotechnol.* **14**, 586 (2019).
24. Wolters, J. et al. Simple atomic quantum memory suitable for semiconductor quantum dot single photons. *Phys. Rev. Lett.* **119**, 060502 (2017).
25. Neuwirth, J. et al. Quantum dot technology for quantum repeaters: from entangled photon generation toward the integration with quantum memories. *Mater. Quantum Technol.* **1**, 043001 (2021).
26. Thomas, S. E. et al. Deterministic storage and retrieval of telecom light from a quantum dot single-photon source interfaced with an atomic quantum memory. *Sci. Adv.* **10**, eadi7346 (2024).
27. Lu, C.-Y. & Pan, J.-W. Quantum-dot single-photon sources for the quantum internet. *Nat. Nanotechnol.* **16**, 1294 (2021).
28. Yu, Y. et al. Telecom-band quantum dot technologies for long-distance quantum networks. *Nat. Nanotechnol.* **18**, 1389 (2023).
29. Stevenson, R. M. et al. Quantum teleportation of laser-generated photons with an entangled-light-emitting diode. *Nat. Commun.* **4**, 2859 (2013).
30. Nilsson, J. et al. Quantum teleportation using a light-emitting diode. *Nat. Photonics* **7**, 311 (2013).
31. Huwer, J. et al. Quantum-dot-based telecommunication-wavelength quantum relay. *Phys. Rev. Appl.* **8**, 024007 (2017).
32. Reindl, M. et al. All-photonic quantum teleportation using on-demand solid-state quantum emitters. *Sci. Adv.* **4**, eaau1255 (2018).
33. Anderson, M. et al. Quantum teleportation using highly coherent emission from telecom C-band quantum dots. *npj Quantum Inf.* **6**, 14 (2020).
34. Anderson, M. et al. Gigahertz-clocked teleportation of time-bin qubits with a quantum dot in the telecommunication C band. *Phys. Rev. Appl.* **13**, 054052 (2020).
35. Basso Basset, F. et al. Entanglement swapping with photons generated on demand by a quantum dot. *Phys. Rev. Lett.* **123**, 160501 (2019).

36. Zopf, M. et al. Entanglement swapping with semiconductor-generated photons violates Bell's inequality. *Phys. Rev. Lett.* **123**, 160502 (2019).
37. Basso Basset, F. et al. Quantum teleportation with imperfect quantum dots. *npj Quantum Inf.* **7**, 7 (2021).
38. Gao, W. B. et al. Quantum teleportation from a propagating photon to a solid-state spin qubit. *Nat. Commun.* **4**, 2744 (2013).
39. Delteil, A. et al. Generation of heralded entanglement between distant hole spins. *Nat. Phys.* **12**, 218 (2016).
40. Bennett, A. J., Patel, R. B., Nicoll, C. A., Ritchie, D. A. & Shields, A. J. Interference of dissimilar photon sources. *Nat. Phys.* **5**, 715 (2009).
41. Weber, J. H. et al. Two-photon interference in the telecom C-band after frequency conversion of photons from remote quantum emitters. *Nat. Nanotechnol.* **14**, 23 (2019).
42. Schimpf, C. et al. Quantum dots as potential sources of strongly entangled photons: perspectives and challenges for applications in quantum networks. *Appl. Phys. Lett.* **118**, 100502 (2021).
43. You, X. et al. Quantum interference with independent single-photon sources over 300 km fiber. *Adv. Photonics* **4**, 066003 (2022).
44. Santori, C., Fattal, D., Vuckovic, J., Solomon, G. S. & Yamamoto, Y. Indistinguishable photons from a single-photon device. *Nature* **419**, 594 (2002).
45. Ates, S. et al. Post-selected indistinguishable photons from the resonance fluorescence of a single quantum dot in a microcavity. *Phys. Rev. Lett.* **103**, 167402 (2009).
46. Gazzano, O. et al. Bright solid-state sources of indistinguishable single photons. *Nat. Commun.* **4**, 1425 (2013).
47. Bayer, M. et al. Fine structure of neutral and charged excitons in self-assembled In (Ga) As/(Al) GaAs quantum dots. *Phys. Rev. B* **65**, 195315 (2002).
48. Trotta, R. et al. Universal recovery of the energy-level degeneracy of bright excitons in InGaAs quantum dots without a structure symmetry. *Phys. Rev. Lett.* **109**, 147401 (2012).
49. Huber, D. et al. Strain-tunable GaAs quantum dot: a nearly dephasing-free source of entangled photon pairs on demand. *Phys. Rev. Lett.* **121**, 033902 (2018).
50. Wang, H. et al. On-demand semiconductor source of entangled photons which simultaneously has high fidelity, efficiency, and indistinguishability. *Phys. Rev. Lett.* **122**, 113602 (2019).
51. Rota, M. B. et al. A source of entangled photons based on a cavity-enhanced and strain-tuned GaAs quantum dot. *eLight* **4**, 13 (2024).
52. Basso Basset, F. et al. Quantum key distribution with entangled photons generated on demand by a quantum dot. *Sci. Adv.* **7**, eabe6379 (2021).
53. Basso Basset, F. et al. Daylight entanglement-based quantum key distribution with a quantum dot source. *Quantum Sci. Technol.* **8**, 025002 (2023).
54. Jayakumar, H. et al. Deterministic photon pairs and coherent optical control of a single quantum dot. *Phys. Rev. Lett.* **110**, 135505 (2013).
55. Müller, M., Bounouar, S., Jöns, K. D., Glässl, M. & Michler, P. On-demand generation of indistinguishable polarization-entangled photon pairs. *Nat. Photonics* **8**, 224 (2014).
56. Gurioli, M., Wang, Z., Rastelli, A., Kuroda, T. & Sanguinetti, S. Droplet epitaxy of semiconductor nanostructures for quantum photonic devices. *Nat. Mater.* **18**, 799 (2019).
57. Schliwa, A., Winkelnkemper, M. & Bimberg, D. Few-particle energies versus geometry and composition of $In_xGa_{1-x}As/GaAs$ self-organized quantum dots. *Phys. Rev. B* **79**, 075443 (2009).
58. Legero, T., Wilk, T., Hennrich, M., Rempe, G. & Kuhn, A. Quantum beat of two single photons. *Phys. Rev. Lett.* **93**, 070503 (2004).
59. Schöll, E. et al. Crux of using the cascaded emission of a three-level quantum ladder system to generate indistinguishable photons. *Phys. Rev. Lett.* **125**, 233605 (2020).
60. Bouwmeester, D. et al. Experimental quantum teleportation. *Nature* **390**, 575 (1997).
61. Rota, M. B., Basset, F. B., Tedeschi, D. & Trotta, R. Entanglement teleportation with photons from quantum dots: toward a solid-state based quantum network. *IEEE J. Sel. Top. Quantum Electron.* **26**, 1 (2020).
62. Chuang, I. L. & Nielsen, M. A. Prescription for experimental determination of the dynamics of a quantum black box. *J. Mod. Opt.* **44**, 2455 (1997).
63. Massar, S. & Popescu, S. Optimal extraction of information from finite quantum ensembles. *Phys. Rev. Lett.* **74**, 1259 (1995).
64. Valivarthi, R. et al. Quantum teleportation across a metropolitan fibre network. *Nat. Photonics* **10**, 676 (2016).
65. Sun, Q.-C. et al. Quantum teleportation with independent sources and prior entanglement distribution over a network. *Nat. Photonics* **10**, 671 (2016).
66. Valivarthi, R. et al. Teleportation systems toward a quantum internet. *PRX Quantum* **1**, 020317 (2020).
67. Zhao, J. Enhancing quantum teleportation efficacy with noiseless linear amplification. *Nat. Commun.* **14**, 4745 (2023).
68. Strobel, T. et al. Quantum teleportation with telecom photons from remote quantum emitters, *arXiv preprint* https://doi.org/10.48550/arXiv.2411.12904 (2024).
69. Kuhlmann, A. V. et al. Transform-limited single photons from a single quantum dot. *Nat. Commun.* **6**, 8204 (2015).
70. Efros, A. L. & Nesbitt, D. J. Origin and control of blinking in quantum dots. *Nat. Nanotechnol.* **11**, 661 (2016).
71. Undeutsch, G. et al. Electric-field control of photon indistinguishability in cascaded decays in quantum dots. *Nano Lett.* **25**, 7121 (2025).
72. Kambs, B. & Becher, C. Limitations on the indistinguishability of photons from remote solid state sources. *N. J. Phys.* **20**, 115003 (2018).
73. Ghosh, S. et al. Distinguishability of Bell states. *Phys. Rev. Lett.* **87**, 277902 (2001).
74. Barbieri, M., Vallone, G., Mataloni, P. & De, F. Complete and deterministic discrimination of polarization Bell states assisted by momentum entanglement. *Phys. Rev. A* **75**, 042317 (2007).
75. Calsamiglia, J. & Lütkenhaus, N. Maximum efficiency of a linear-optical Bell-state analyzer. *Appl. Phys. B* **72**, 67 (2001).
76. Nielsen, M. A. and Chuang, I. L. *Quantum Computation and Quantum Information* (Cambridge University Press, 2010).
77. Knee, G. C., Bolduc, E., Leach, J. & Gauger, E. M. Quantum process tomography via completely positive and trace-preserving projection. *Phys. Rev. A* **98**, 062336 (2018).

Acknowledgements

This project has received funding from the European Union's Horizon 2020 research and innovation program under Grant Agreement no. 899814, Qurope project (R.T., K.D.J., F.Sc., A.R.) and No. 871130, Ascent+ project (A.R.), and from the QuantERA II program that has received funding from the European Union's Horizon 2020 research and innovation program under Grant Agreement No 101017733 via the project QD-E-QKD (R.T., F.B.B., N.S., T.H.L., A.R.) and the FFG grant no. 891366, MEEDGARD project (S.S., A.R.). The authors also acknowledge support from MUR (Ministero dell'Università e della Ricerca) through the PNRR MUR project PE0000023-NQSTI (R.T., F.B.B, F.Sc.), the European Union's Horizon Europe research and innovation program under EPIQUE Project GA No. 101135288 (R.T., N.S., F.Sc.), and the European Commission by project QUID (Quantum Italy Deployment) funded in the Digital Europe Programme under the grant agreement No 101091408 (R.T., N.S., and F.Sc.). This work is supported by the Deutsche Forschungsgemeinschaft (German Research Foundation) through the transregional collaborative research center TRR142/3-2022 (231447078) (K.D.J.) and the European Research Council starting grant (LiNQs, 101042672) (K.D.J.). A. R.

acknowledges support from the Austrian Science Fund FWF via the Research Group FG5, the cluster of excellence quantA [10.55776/COE1], the Linz Institute of Technology (LIT), the LIT Secure and Correct Systems Lab, supported by the State of Upper Austria. T.H.L. acknowledges funding from the German ministry of research, technology and space (BMFTR) for the project Qecs (FKZ: 13N16272). S.H. acknowledges funding from the German ministry of research, technology and space (BMFTR) within the project QR.N (FKZ: 16KIS2209). S.F.C.d.S. acknowledges São Paulo Research Foundation (FAPESP), Brasil, Process Number 2024/08527-2 and 2024/21615-8 for financial support. The authors thank Paolo Mataloni for useful discussion.

Author contributions

A.L., G.R., M.B., G.D., and M.B.R. performed the experiment over the fiber network under the supervision of F.B.B. and R.T. A.L., G.R., M.B., G.D., and M.B.R. performed the experiment over the hybrid network on the Marconi side of the free-space channel under the supervision of F.B.B. and R.T. P.B. and A.S. participated to the experiment on the Fermi side of the free-space channel under the supervision of G.C., N.S. and F.Sc. F.Sa., N.C.R. and K.D.J. contributed to the experimental setup implementation. F.Sa. and P.B. developed the data acquisition code with supervision of F.B.B., A.L., K.J., N.S., G.C., and F.Sc. A.L., G.R., M.B. and G.D. analyzed the data. F.B.B. developed the model for the expected quantum teleportation performances. L.C. contributed to the setup and characterization of the free-space channel. E.S., L.H., J.N. performed preliminary experiments and studies under the supervision of K.D.J. and R.T. S.F.C.d.S. and A.R. designed and grew the QD sample. M.B.R., T.M.K. and Q.B. designed and processed the cavity of the QD with the supervision of R.T., A.R., T.H.L. and S.H. S.S. processed the micro-machined piezoelectric actuator. M.A.U.C. developed the fast single-photon detectors for the experiments. A.L. and R.T. wrote the paper with contribution from all the authors. R.T. conceived the experiment. A.R., F.Sc., K.D.J. and R.T. coordinated the project.

Competing interests

The authors declare no competing interests.

Additional information

Supplementary information The online version contains supplementary material available at https://doi.org/10.1038/s41467-025-65911-9.

Correspondence and requests for materials should be addressed to Alessandro Laneve or Rinaldo Trotta.

Peer review information *Nature Communications* thanks Pawel Holewa and the other, anonymous, reviewer(s) for their contribution to the peer review of this work.

[1]Dipartimento di Fisica, Sapienza Università di Roma, Roma, Italy. [2]Institute for Photonic Quantum Systems (PhoQS), Center for Optoelectronics and Photonics Paderborn (CeOPP) and Department of Physics, Paderborn University, Paderborn, Germany. [3]Institute of Semiconductor and Solid State Physics, Johannes Kepler University, Linz, Austria. [4]TUM School of Computation, Information and Technology, Technical University of Munich, Garching 85748, Germany. [5]Technische Physik, University of Würzburg, Am Hubland, Würzburg, Germany. [6]Universidade Estadual de Campinas, Instituto de Física Gleb Wataghin, Campinas, Brazil. [7]Research Centre for Microtechnology FHV—Vorarlberg University of Applied Sciences Hochschulstraße 1, Dornbirn, Austria. [8]Institute of Photonics and Quantum Electronics, Karlsruhe Institute of Technology, Karlsruhe, Germany. [9]Center for Integrated Quantum Science and Technology (IQST), Karlsruhe Institute of Technology, Karlsruhe, Germany. [10]Single Quantum B.V., Delft, The Netherlands. [11]Dipartimento di Fisica, Politecnico di Milano, Milano, Italy. ✉e-mail: alessandro.laneve@uniroma1.it; rinaldo.trotta@uniroma1.it